A non-oscillatory staggered grid algorithm for the pressure-displacement coupling in geomechanics

Clovis R. Maliska*, Hermínio T. Honório* and Jurandir Coelho Jr.*

* Federal University of Santa Catarina
Mechanica Engineering Department
SINMEC - Computational Fluid Dynamics Laboratory
88040-900 - Florianópolis-SC-Brazil
maliska@sinmec.ufsc.br
herminio.eng@gmail.com
jurandir@sinmec.ufsc.br

ABSTRACT

This paper investigates a new finite volume alternative for solving coupled poromechanics by employing a staggered arrangement for pressure and displacements over an unstructured grid. By staggering these variables, an improvement is obtained for the pressure-displacement coupling, which is claimed by the authors to prevent the numerical solution from instabilities. The two-dimensional formulation is still under development, thus, results are presented only for the one-dimensional case. Both collocated and staggered arrangements are compared with analytical solutions and the results are very promising, indicating that staggering the rock displacements related to the pressure is a viable approach to confer robustness to the numerical scheme.

1 Introduction

Several engineering problems are modeled by systems of coupled partial differential equations, many of them involving different physics. In geomechanics, in which compacting porous media is coupled with the fluid flow, is one example. In this case, a delicate coupling between pore-pressure and rock displacement is present, since under certain conditions, as in the very beginning of the transient, or at the interface of two materials with different permeability, pressure wiggles appear in the numerical solution. Those situations, which resemble an undrained condition, impose an almost zero compressibility, which creates the condition for this pathology to appear for certain numerical approximations. In the class of Finite Element methods, extensively used for solving the rock mechanics in porous media, several remedies for this pathology are available, being mixed finite element [1] and discontinuous Galerkin some of the possibilities. However, those remedies are at a cost of considerably increasing the computer time. Alternatively, some authors have [2, 3] proposed stabilization techniques that do not increase the computational cost and still eliminate the instabilities, but at a cost of introducing numerical diffusion to the solution. Recently, in the context of finite volumes, Honório and Maliska [4] have proposed a strategy for avoiding such instabilities which can be also regarded as a stabilization technique. In spite of all these alternatives, a numerical scheme that efficiently eliminates the pressure wiggles without introducing numerical diffusion and increasing computational cost, while keeping the same order of accuracy for both pressure and displacements is still pursued.

An analysis of the coupling between pressure and displacement for poroelasticity, and pressure and velocity for Navier-Stokes flows, reveals that they are of the same nature, so it is expected that the remedies employed in one class of problems can be applied to the other one with success. With this in mind, the oscillatory pressure fields arising when solving incompressible Navier-Stokes flows is known for more than four decades, and can be fully mitigated if a staggered grid approach is employed [5]. This remedy was abandoned when unstructured grids were required for solving fluid flows in complex geometries, due to the alleged complexity of implementation. This paper addresses this issue, advancing a finite volume method using unstructured grids with staggered

variables, avoiding the oscillatory pressure field in geomechanics [6].

First, we present the mathematical model for coupled poromechanics. Then, the fundamentals of the staggered arrangement of variables is discussed and a brief analogy is established between pressure-displacement in poromechanics and pressure-velocity in the Navier-Stokes equations. The model equations are discretized for two-dimensions and possible alternatives are suggested. In the sequence, a one-dimensional discretization is performed for both staggered and collocated arrangements and some preliminary results are presented. Finally, a few remarks close the presentation.

2 Mathematical Model

The mechanical behavior of saturated porous media is affected by its mechanical properties and the pressure of the fluid filling its pores. Terzaghi [7] introduced the concept of effective stress into the equations of stress equilibrium in order to take the pore pressure into account, yielding to:

$$\nabla \cdot \boldsymbol{\sigma} - \alpha \nabla p = \mathbf{b}, \tag{1}$$

where ∇ is the nabla operator, $\boldsymbol{\sigma}$ is the effective stress tensor, α is the Biot coefficient, p is the pore pressure and $\mathbf{b}$ is a source term. Moreover, considering small strains and a stress-strain relationship represented by the constitutive matrix $\mathbb{C}$ (Voigt notation), the effective stress tensor can be written in terms of the displacement vector $\mathbf{u}$ by the expression:

$$\boldsymbol{\sigma} = \mathbb{C} \nabla_s \mathbf{u}, \tag{2}$$

with ∇_s being the symmetric nabla operator.

The closure of the model is ensured by the mass conservation equation for deformed porous media:

$$\frac{1}{M}\frac{\partial \hat{p}}{\partial t} + \nabla \cdot \left(\mathbf{v}^f + \alpha \mathbf{v}^s \right) = q, \tag{3}$$

in which $1/M$ is the Biot module and q is a source term. Equation (3) is conveniently written here in terms of the fluid velocity, $\mathbf{v}^f$, and the solid grains velocity, $\mathbf{v}^s$, which are respectively given by:

$$\mathbf{v}^f = -\frac{\mathbf{k}}{\mu} \nabla p, \tag{4}$$

$$\mathbf{v}^s = \frac{\partial \mathbf{u}}{\partial t}. \tag{5}$$

with $\mathbf{k}$ being the absolute permeability tensor and μ the fluid viscosity. The gravitational term in equation (4) has been neglected with no loss of generality.

3 Staggered Arrangement

One of the major challenges faced by the numerical schemes developed to solve equations (1) and (3) is how to avoid pressure wiggles that can appear under undrained consolidation. In this situation the consolidation process takes place in a much smaller time scale than the fluid motion ($\mathbf{v}^s >> \mathbf{v}^f$), which yields to the following mass conservation equation:

$$\frac{1}{M}\frac{\partial p}{\partial t} + \alpha \nabla \cdot \mathbf{v}^s = q. \tag{6}$$

Equation (6) is very similar to the mass conservation equation that appears when solving the Navier-Stokes equations for compressible flows. It is well known that properly satisfying this equation is of utmost importance to avoid the checkerboard pressure problem [8]. Recalling equation (5), the problem here resides on how to determine a displacement field that fully satisfy both mass and

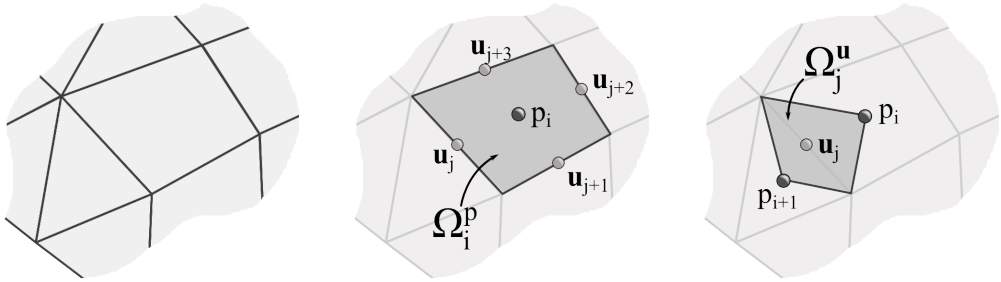

Figure 1: Geometrical entities: (a) computer mesh composed by triangular and quadrilateral elements; (b) control volume for mass conservation with p_i stored at its centroid; and (c) control volume built around displacement vector $\mathbf{u}_j$ for momentum equilibrium.

momentum equations. For the Navier-Stokes equations the problem is exactly the same, except that the unknown variable is the velocity field instead of displacement.

Ensuring mass and momentum conservation is not a trivial task to be accomplished. The first solution to this problem was proposed by Harlow and Welch [5], in the context of finite differences, where they staggered the positions of pressure and velocities. In this manner, these two variables are directly available where they are required during the discretization of the differential equations. This technique is recognized to completely mitigate pressure wiggles for the Navier-Stokes equations. Due to the similarity of equation (6), stated in the previous paragraph, a staggered arrangement between pressure and displacement might have good chances to show a good performance for geomechanics as well.

4 Finite Volume Formulation

The traditional procedure for obtaining the approximate equations by the finite volume method starts by simply integrating the differential equations over each control volume of the grid. Since we propose a staggered arrangement of control volumes for $\mathbf{u}$ and p, a clear definition of these geometrical entities is now of interest. In this work, we follow the methodology presented by Peters and Maliska [9] for building staggered control volumes on unstructured grids.

In figure (1a) it is shown the base mesh provided by the grid generator. As depicted in figure (1b) for p_i, the control volumes for mass conservation, Ω^p, coincides with the elements of the base mesh. For the momentum equilibrium, however, the control volumes, $\Omega^{\mathbf{u}}$, are built around the edges of the elements by connecting the vertices of the edge with the centroids of the two adjacent elements. A control volume $\Omega^{\mathbf{u}}$ is represented in figure (1c) and the position of $\mathbf{u}_j$ is at the midpoint of the edge. The key point of this configuration is that the displacements are located at the faces of the control volume Ω^p (figure (1b)), which will have a direct impact on the volumetric strain computation over Ω^p, as shown later. Now we proceed with the discretization of the differential equations.

4.1 Mass conservation equation

Equation (3) is first integrated over a time step, Δt, along with an implicit first-order backward Euler scheme. The remaining equation is then integrated over the control volume Ω_i^p, and the divergence theorem is applied to obtain the surface integrals. By the midpoint rule, the semi-discretized form of equation (3) is:

$$\frac{\Delta\Omega_i^p}{M}\frac{p_i}{\Delta t} + \sum_{ip\in\Gamma_i^p}\Big[(\mathbf{v}^f + \alpha\mathbf{v}^s)\cdot\mathbf{s}\Big]_{ip} = q_i\Delta\Omega_i^p + \frac{\Delta\Omega_i^p}{M}\frac{p_i^o}{\Delta t}, \tag{7}$$

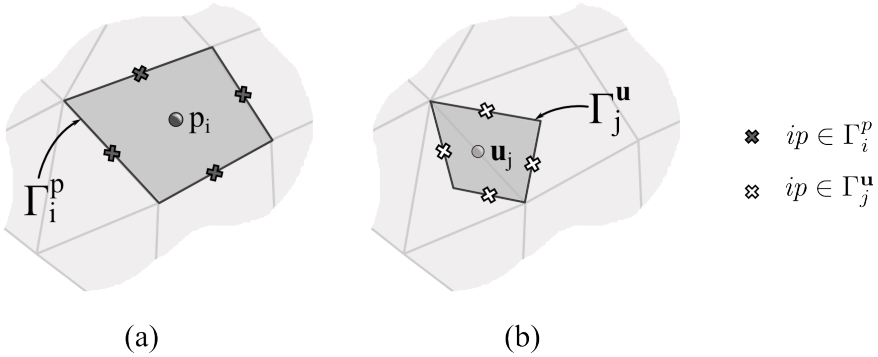

Figure 2: Integration points belonging to the control surfaces (a) Γ_i^p and (b) $\Gamma_j^{\mathbf{u}}$ associated to Ω_i^p and $\Omega_j^{\mathbf{u}}$, respectively.

in which the variables evaluated at the previous time level take the superscript ^{o}, and no superscript is used otherwise. Each control volume Ω^p is bounded by a set of faces (or edges) and at the midpoint of each face is located an integration point ip. The set of integration points surrounding Ω_i^p is denoted by Γ_i^p, as highlighted in figure (2). Each integration point has an area vector, $\mathbf{s}_{ip}$, pointing outwards the control volume. In addition, the volume of Ω^p is represented by $\Delta\Omega^p$.

Recalling equation (5), the mass fluxes crossing the faces of Ω^p due to the rock deformation and fluid motion are respectively given by:

$$w_{ip}^s = (\mathbf{v}^s \cdot \mathbf{s})_{ip} = \frac{(\mathbf{u}_{ip} - \mathbf{u}_{ip}^o)}{\Delta t} \cdot \mathbf{s}_{ip}, \qquad \forall ip \in \Gamma_i^p, \tag{8}$$

$$w_{ip}^f = (\mathbf{v}^f \cdot \mathbf{s})_{ip} = -\frac{1}{\mu}(\mathbf{k}\nabla p)_{ip} \cdot \mathbf{s}_{ip}, \qquad \forall ip \in \Gamma_i^p. \tag{9}$$

The main advantage of staggering Ω^p and $\Omega^{\mathbf{u}}$ is made clear in equation (8) by noting that the displacement vectors $\mathbf{u}_{ip}$ and $\mathbf{u}_{ip}^o$ are directly available at the integration points of Γ_i^p (see figure (2)), dispensing any kind of interpolation. The benefits of this feature is of particular importance during undrained consolidation (equation (6)), where the mass fluxes through the control volume's faces is entirely given by w^s. This is precisely the point we claim to be key for avoiding the pressure instabilities.

The next step is to decide how to reconstruct the pressure gradient of equation (9) at the integration points belonging to Γ^p. Cerbato et al. [10] present an extensive analysis of several techniques for gradient reconstruction specifically applied to reservoir simulation, which could be readily applied here to approximate equation (9). Alternatively, the mass fluxes w^f could be also evaluated by a Multi-Point Flux Approximation (MPFA), as proposed by Aavastmark et al. [11], which would be of particular interest since this methodology is already employed by most of the commercial reservoir simulators.

4.2 Momentum equilibrium equations

Equation (1) is integrated over the control volume $\Omega_j^{\mathbf{u}}$, as depicted in figure (1c), and the divergence theorem is applied to the divergent operator yielding to:

$$\sum_{ip \in \Gamma_j^{\mathbf{u}}} (\boldsymbol{\sigma} \cdot \bar{\mathbf{s}})_{ip} - \alpha \int_{\Omega_j^{\mathbf{u}}} \nabla p \, \mathrm{d}\Omega_j^{\mathbf{u}} = \mathbf{b}_j \Delta\Omega_j^{\mathbf{u}}, \tag{10}$$

where $\Gamma_j^{\mathbf{u}}$ is the set of integration points surrounding $\Omega_j^{\mathbf{u}}$, as shown in figure (2b), and $\bar{\mathbf{s}}$ is an appropriate arrangement of the area vector components, which for the two-dimensional case is:

$$\bar{\mathbf{s}} = \begin{bmatrix} s_x & 0 \\ 0 & s_y \\ s_y & s_x \end{bmatrix}. \tag{11}$$

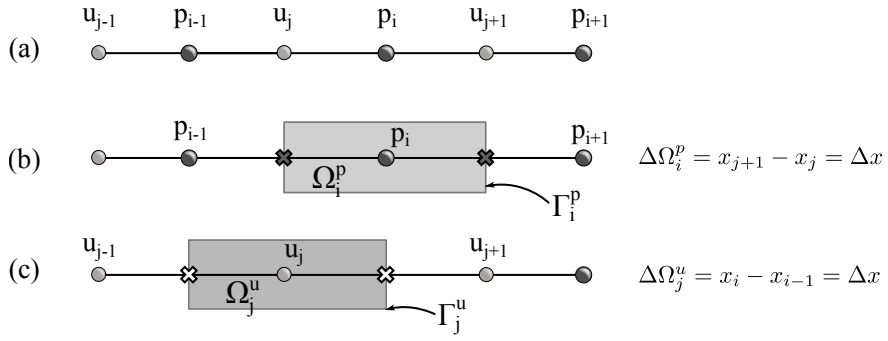

Figure 3: Staggered control volumes associated to a one-dimensional grid with unitary cross section area.

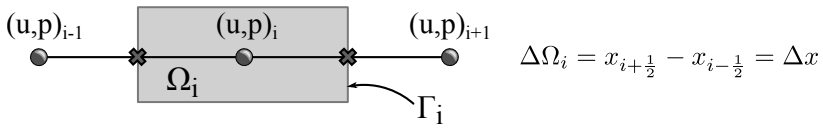

Figure 4: Collocated control volumes associated to a one-dimensional grid with unitary cross section area. Obs: Ω_i indicates that $\Omega_i^p = \Omega_i^u$

The volumetric integral of the pressure gradient in equation (10) is approximated by the Green Gauss theorem:

$$\int_{\Omega_j^{\mathbf{u}}} \nabla p \, \mathrm{d}\Omega_j^{\mathbf{u}} \approx \nabla p_j \Delta\Omega_j^{\mathbf{u}}. \tag{12}$$

Now, it is important to notice that ∇p_j is exactly the same as the pressure gradient required by equation (9), since a displacement position j always coincide with an integration point belonging to Γ_i^p, as it can be observed in figure (2). Therefore, the methodology chosen to evaluate equation (9) can be the same used to compute equation (12).

The remaining term in equation (10) to be evaluated is the stress tensor, $\boldsymbol{\sigma}_{ip}$, at the integration point belonging to $\Gamma_j^{\mathbf{u}}$. This is done by equation (2), but the point is how to compute the displacement derivatives, $\nabla_s \mathbf{u}$, at the integration points of $\Gamma_j^{\mathbf{u}}$. In [9] it is presented the procedure to compute velocity derivatives at these positions, which will be also applied here for computing $\nabla_s \mathbf{u}$.

5 One-Dimensional Formulation

In this work we present some preliminary results of the above formulation applied to the particular case of one-dimensional consolidation, where the grid shown in figure (3) can be employed. The results are compared with the traditional collocated arrangement of variables, as the grid depicted in figure (4). Both strategies are briefly described below.

5.1 Staggered formulation

Integrating equations (3) and (1) over Ω_i^p and Ω_j^u of figure (3), respectively, results in:

$$\frac{\Delta\Omega_i^p}{M}\frac{p_i}{\Delta t} - \frac{k}{\mu}\left(\left.\frac{\partial p}{\partial x}\right|_{j+1} - \left.\frac{\partial p}{\partial x}\right|_{j}\right) + \frac{\alpha}{\Delta t}\left(u_{j+1} - u_j\right) = \frac{\Delta\Omega_i^p}{M}\frac{p_i^o}{\Delta t} - \frac{\alpha}{\Delta t}\left(u_{j+1}^o - u_j^o\right), \tag{13}$$

$$\sigma_i - \sigma_{i-1} - \alpha\left(p_i - p_{i-1}\right) = 0, \tag{14}$$

with the following approximations at the integration points,

$$\left.\frac{\partial p}{\partial x}\right|_{j+1} \approx \frac{p_{i+1}-p_i}{\Delta x}, \tag{15}$$

$$\left.\frac{\partial p}{\partial x}\right|_{j} \approx \frac{p_i-p_{i-1}}{\Delta x}, \tag{16}$$

$$\sigma_i \approx \frac{E}{\Delta x}\left(u_{j+1}-u_j\right), \tag{17}$$

$$\sigma_{i-1} \approx \frac{E}{\Delta x}\left(u_j-u_{j-1}\right). \tag{18}$$

The set of equations (13) and (14), along with the approximations (15-18), composes a linear system of equations that is solved in a monolithic fashion. The results of these equations are presented in the next section.

5.2 Collocated formulation

The discretization of the equations for a collocated grid is basically the same as the previous case, except that the integration is performed over the same control volume Ω_i. In this manner, the resultant equations are:

$$\frac{\Delta\Omega_i}{M}\frac{p_i}{\Delta t}-\frac{k}{\mu}\left(\left.\frac{\partial p}{\partial x}\right|_{i+\frac{1}{2}}-\left.\frac{\partial p}{\partial x}\right|_{i-\frac{1}{2}}\right)+\frac{\alpha}{\Delta t}\left(u_{i+\frac{1}{2}}-u_{i-\frac{1}{2}}\right)=\frac{\Delta\Omega_i^p}{M}\frac{p_i^o}{\Delta t}-\frac{\alpha}{\Delta t}\left(u^o_{i+\frac{1}{2}}-u^o_{i-\frac{1}{2}}\right), \tag{19}$$

$$\sigma_{i+\frac{1}{2}}-\sigma_{i-\frac{1}{2}}-\alpha\left(p_{i+\frac{1}{2}}-p_{i-\frac{1}{2}}\right)=0, \tag{20}$$

The usual approximations at the integration points still hold:

$$\left.\frac{\partial p}{\partial x}\right|_{i+\frac{1}{2}} \approx \frac{p_{i+1}-p_i}{\Delta x}, \tag{21}$$

$$\left.\frac{\partial p}{\partial x}\right|_{i-\frac{1}{2}} \approx \frac{p_i-p_{i-1}}{\Delta x}, \tag{22}$$

$$\sigma_{i+\frac{1}{2}} \approx \frac{E}{\Delta x}\left(u_{i+1}-u_i\right), \tag{23}$$

$$\sigma_{i-\frac{1}{2}} \approx \frac{E}{\Delta x}\left(u_i-u_{i-1}\right). \tag{24}$$

In addition, the pressure and displacement are required at positions $x_{i-\frac{1}{2}}$ and $x_{i+\frac{1}{2}}$, where they are not available. In this case, we use a second-order approximation, so,

$$p_{i+\frac{1}{2}} \approx \frac{p_{i+1}-p_i}{2}, \tag{25}$$

$$p_{i-\frac{1}{2}} \approx \frac{p_i-p_{i-1}}{2}, \tag{26}$$

$$u_{i+\frac{1}{2}} \approx \frac{u_{i+1}-u_i}{2}, \tag{27}$$

$$u_{i-\frac{1}{2}} \approx \frac{u_i-u_{i-1}}{2}. \tag{28}$$

6 Preliminary Results

In this section, a one-dimensional consolidation problem is solved. As depicted in figure (5), the domain has its bottom boundary fixed and impermeable and the top boundary fully-permeable

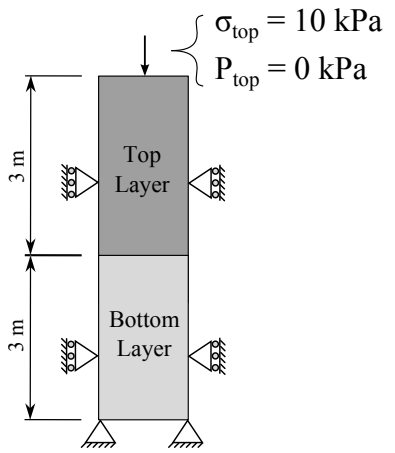

Figure 5: Geometry and boundary conditions for the one-dimensional consolidation problem.

(p_{top} =0 kPa) and subjected to a compressive load of σ_{top} =10 kPa. The structure is initially undeformed and the initial pore-pressure equals to zero. The fluid phase properties is taken as those of water at 20^{o}C, that is, $\rho = 998.2$ kg/m^3, $\mu = 1.002 \times 10^{-3}$ Pa·s and $c_f = 4.59 \times 10^{-4}$ MPa^{-1}. The solid phase can be composed either by two different materials, as indicated in figure (5), or only one material. The geomechanical properties of the materials considered in this work are summarized in table (1), where K stands for the hydraulic conductivity.

Table 1: Solid phase properties.

	Sand	Silty Clay
K (m/s)	1×10^{-4}	5×10^{-9}
E (MPa)	4.503	2.129
c_s (MPa^{-1})	0.0	0.0
ϕ	0.3	0.3
α	1.0	1.0

6.1 Verification

In order to verify the correct implementation of the algorithms, it is considered the case in which the column is composed by sand only. This problem presents analytical solution for both pressure and displacement fields, which allows us to have a visual comparison of the results obtained by the proposed staggered arrangement as well as the collocated one. With a fixed time step of 0.1 second, the pressure and displacement profiles along the vertical direction are plotted in figures (6a) and (6b) for four time levels. As it can be seen, both formulations are in good agreement with the analytical solutions.

6.2 Convergence Analysis

Now, we consider a set of progressively refined grids and take the pressure and displacement profiles at $t = 700$ seconds, as shown in figure (6). We compare these profiles with the analytical solution and compute the Euclidean norm (L_2-norm) of the error vector for each one of the grids and for three different time steps. By this procedure we can evaluate the order of convergence of each variable. The results obtained are shown in figures (7) and (8) for the staggered and collocated formulations,respectively. These figures show second-order accuracy for both pressure and displacement for both formulations.

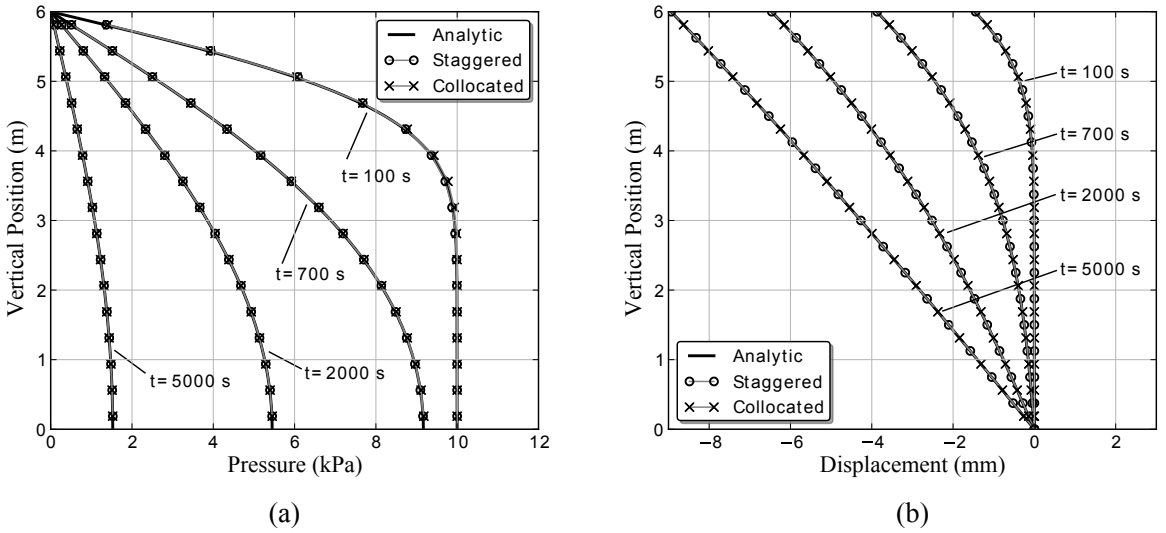

Figure 6: Staggered control volumes associated to a one-dimensional grid. Obs: the cross section area is considered to be the unity.

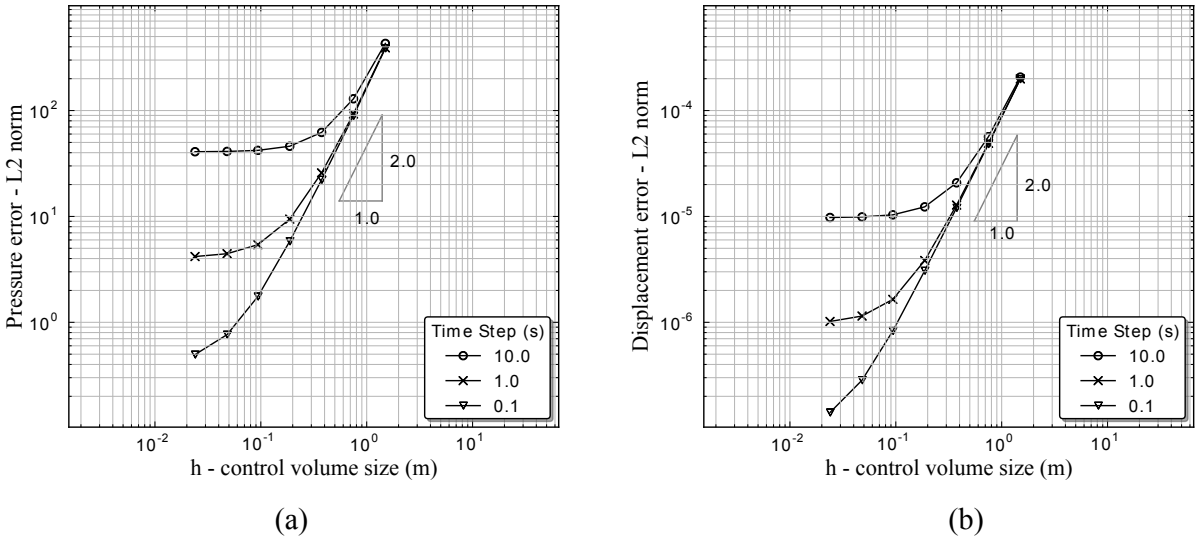

Figure 7: Convergence analysis of (a) pressure and (b) displacement fields for the staggered arrangement of variables.

6.3 Pressure Instabilities

Up to now, the results showed quite similar behaviour for both formulations. However, if we induce an undrained consolidation, pressure instabilities are expected to appear in the numerical solution. One way of obtaining this situation is by reducing the time step enough to violate the minimum time step criteria postulated by Vermeer and Verruijt [12]. Basically, this criteria depends on the poromechanical properties and the grid spacing. This means that any pressure instability can be removed by simply refining the grid, but this can often compromise computational performance for real applications.

Considering the same problem as before and reducing the time step to 0.001 second, the pressure profiles obtained at $t = 1.0$ second by the collocated and the staggered formulations are shown in figures (9a) and (9b) for a grid composed by 8 and 16 nodes of pressure, respectively. It can be seen in figure (9a) that the pressure instabilities spread through the entire domain, while they are more concentrated at the top boundary as the grid is refined (figure (9b)), suggesting that the

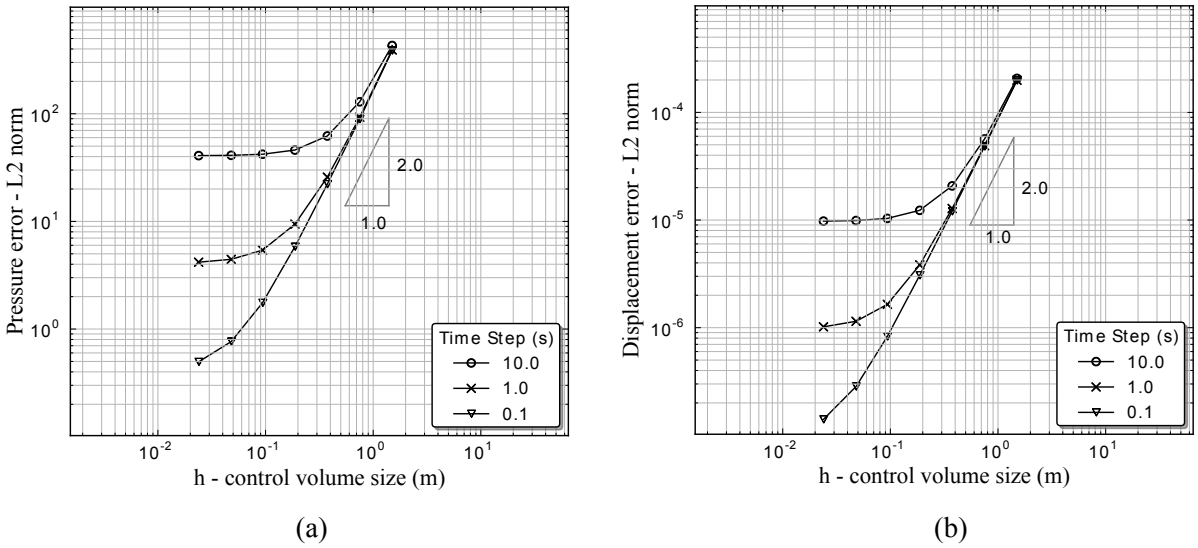

Figure 8: Convergence analysis of (a) pressure and (b) displacement fields for the collocated arrangement of variables.

instabilities indeed tends to vanish as the grid is refined. On the other hand, the same figure (9) shows no instabilities at all for the pressure profiles obtained by staggered formulation, irrespective to the grid refinement.

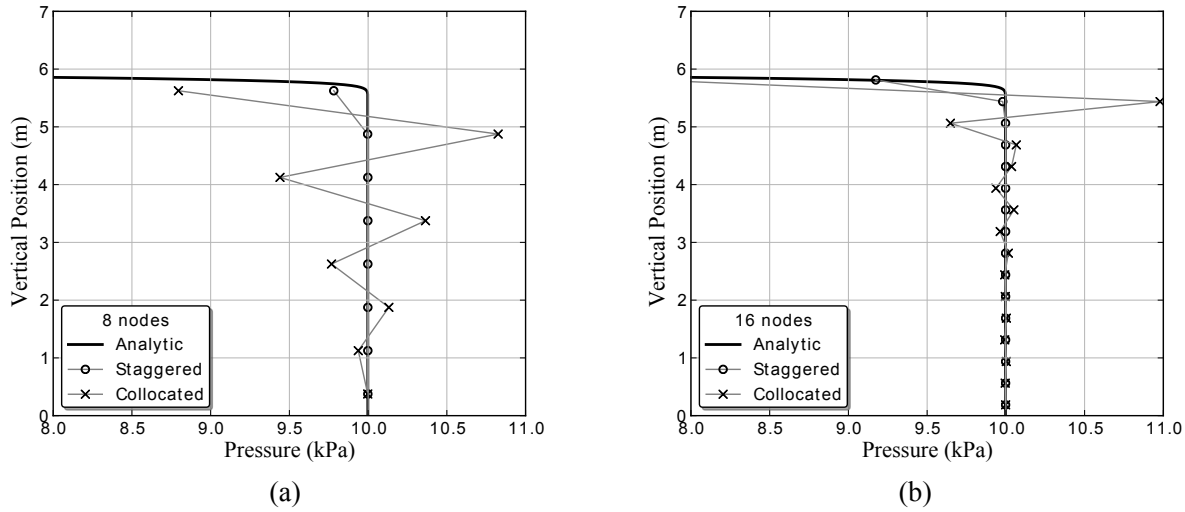

Figure 9: Pressure profiles under undrained consolidation.

Another way of inducing undrained consolidation is by considering the column composed by two materials with different permeabilities. In this case, the top and bottom layers of figure (5) are considered to be sand and silty-clay, respectively. This problem has analytical solution for the pressure profile and its comparison with the collocated and staggered formulations are shown in figure (10). The time step used is of 0.1 second and the solution was taken at $t = 500$ seconds for a 20 nodes grid. In this case, pronounced pressure oscillations appear along the bottom layer for the collocated arrangement, which seems to also have an impact at the pressure profile along the upper layer. Again, notorious agreement with the analytical solution can be verified for the staggered arrangement, even near the interface between the two regions.

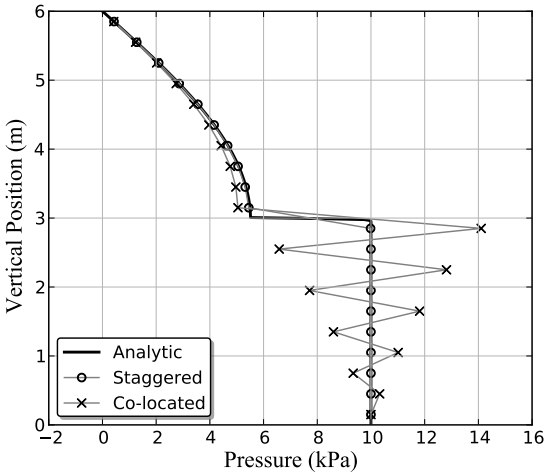

Figure 10: Pressure profiles for the upper and bottom layers of the column composed by sand and silty-clay, respectively.

7 Final Remarks

In this work, a two-dimensional finite volume formulation has been presented for discretizing the coupled poromechanics equations in staggered grids. Preliminary results for the one-dimensional case have shown that the staggered arrangement completely removed the pressure instabilities without introducing any numerical diffusion to the solution. At the same time, second order accuracy has been verified for both pressure and displacement. This leads to believe that the proposed staggered arrangement for unstructured grids is a promising strategy for solving coupled poromechanics in two and three-dimensions.

REFERENCES

[1] Ferronato, M., Castelletto, N. and Gambolati, G. A fully coupled 3-d mixed finite element model of Biot consolidation, *J. of Comp. Phys.*, Vol. **229**, pp. 4813–4830, (2010).

[2] Choo, J. and Borja, R.I. A stabilized mixed finite elements for deformable porous media with double porosity, *Computer Methods in Applied Mechanics and Engineering*, Vol. **293**, pp. 131–154, (2015).

[3] Preisig, M. and Prévost, J.H. Stabilization procedures in coupled poromechanics problems: A critical assessment, *International Journal for Numerical and Analytical Methods in Geomechanics*, Vol. **35**, pp. 1207–1225, (2011).

[4] Honorio, H.T. and Maliska, C.R. A stabilized finite volume method for solving one-dimensional poroelastic problems, *Rio Oil and Gas*, Expo and Conference 2016 Proceedings. Rio de Janeiro (2016).

[5] Harlow, F.H. and Welch, J.E. Numerical calculation of time-dependent viscous incompressible flow of fluid with free surface, *Phys. of Fluids*, Vol. **8**, pp. 2182–2189, (1965).

[6] dal Pizzol, A. and Maliska, C.R. A finite volume method for the solution of fluid flows coupled with the mechanical behavior of compacting porous media, *Porous Media and its Applications in Science, Engineering and Industry AIP Proc.*, 1453, 205–210, (2012).

[7] K. Terzaghi, Die berechnung der durchlassigkeitsziffer des tones aus dem verlauf der hydrodynamischen spannungsercheinungen. Sitzung berichte. Akademie der Wissenschaften, Wien Mathematiesch-Naturwissenschaftliche Klasse, 1923.

[8] S.V. Patankar. *Numerical Heat Transfer and Fluid Flow*. Hemisphere Publishing Corporation, 1980.

[9] Peters, R. and Maliska, C.R. A staggered grid arrangement for solving incompressible flows with hybrid unstructured meshes, *Numer. Heat Transfer*, Vol. **71**, pp. 50–65, (2017).

[10] Cerbato, G., Hurtado, F.S.V., Silva, A.F.C. and Maliska, C.R. Analysis of gradient reconstruction methods on polygonal grids applied to petroleum reservoir simulation, *15th Brazilian Congress of Thermal Science and Engineering*, Belém. ENCIT Proceedings, 2014.

[11] Aavastmark, I., Barkve, T., Bøe, O. and Mannseth, T. Discretization on unstructured grids for inhomogeneous, anisotropic media. Part I, Derivation of the methods, *SIAM Journal on Scientific Computing*, Vol. **19**, No. 5, pp. 1700–1716, (1998).

[12] Vermeer, P.A. and Verruijt, A. An accuracy condition for consolidation by finite elements, *International Journal of Numerical and Analytical Methods in Geomechanics*, Vol. **5**, pp. 1–14, (1981).